Direct detection of the \approx 8.4 eV internal conversion energy of 229m Th embedded in a superconducting nanowire

Galen O'Neil , Kjeld Beeks , Eric Hudson , Justin Jeet, David Leibrandt , Marion Mallweger , Sae Woo Nam, Nayan Patra , Kjeld Beeks , Eric Hudson , Justin Jeet, David Leibrandt , Marion Mallweger , Sae Woo Nam, Nayan Patra , Kjeld Beeks , Dileep Reddy , National , Stephen B. Schoun , Benedict Seiferle, Christian Schneider , Lars von der Wense , Peter G. Thirolf , Varun Verma , Jun Ye , Benedict Seiferle, Christian Schneider , Lars von der Wense , Peter G. Thirolf , Varun Verma , Jun Ye , Benedict Seiferle, Christian Schneider , Lars von der Wense , Peter G. Thirolf , Varun Verma , Jun Ye , Benedict Seiferle, Achristian Schneider , Lars von der Wense , Peter G. Thirolf , Varun Verma , Jun Ye , Benedict Seiferle, Achristian Schneider , Lars von der Wense , Peter G. Thirolf , Varun Verma , Jun Ye , Benedict Seiferle, Achristian Schoen , Lars von der Wense , Peter G. Thirolf , Varun Verma , Jun Ye , Benedict Seiferle, Achristian Schoen , Lars von der Wense , Peter G. Thirolf , Varun Verma , Jun Ye , Stephen B. Schoun , Benedict Seiferle, Seiferle, Stephen B. Schoun , Benedict Seiferle, Seiferle, Stephen B. Schoun , Sehendict Seiferle, Lars von der Wense , Stephen B. Schoun , Sehendict Seiferle, Lars von der Wense , Stephen Lars von Benedict Seiferle, Seiferle, Lars von der Wense , Stephen B. Schoun , Sehendict Seiferle, Lars von der Wense , Stephen B. Schoun , Stephen B. Schoun , Sehendict Seiferle, Lars von der Wense , Stephen B. Schoun , Stephen Lars von der Wense , Stephen Lars von der Wense , Stephen B. Schoun , Stephen B. Schoun , Stephen B. Schoun , Stephen Lars von der Wense , Stephen B. Schoun , Stephen

(Received 9 May 2025; accepted 21 July 2025; published 25 August 2025)

We report on a direct measurement of the \approx 8.4 eV nuclear excitation energy of the isomeric first-excited state 229m Th via the internal conversion (IC) decay channel. Thermalized and mass-filtered recoiling 229m Th ions from 233 U α decay are delivered to the surface of a superconducting nanowire sensor and become embedded. The ion is neutralized, triggering the IC decay, and the energy released by the IC decay is detected with high quantum efficiency by the nanowire sensor. Energy resolution is enabled by the current dependence of the internal quantum efficiency of the nanowire sensor. The techniques presented here are complementary to light-based detection schemes. The IC decay channel is about eight orders of magnitude faster than the photoemission channel, thus the ability to detect IC decays with high efficiency with superconducting nanowire sensors is likely to be a valuable tool for future 229m Th experiments.

DOI: 10.1103/9v5w-b8k2

I. INTRODUCTION

The isomeric first-excited state of the actinide isotope ²²⁹Th, known as the *thorium isomer* ^{229m}Th, is the energetically lowest-lying isomeric excited nuclear state in the known landscape of nuclear species, about five orders of magnitude lower energy than typical nuclear isomers. A proposed nuclear clock [1] based upon this state could reach a fractional accuracy of 10⁻¹⁹ [2,3]. The use of a nuclear transition would enable the clock to be both less sensitive to magnetic and electric fields, while also being 10⁴–10⁵ more sensitive to potential variations in the fundamental constants like the fine structure constant or the scale parameter of the strong interaction compared to conventional atomic clocks [4–8]. Further applications proposed for a ^{229m}Th-based nuclear clock include (ultralight) dark matter research [9–13] or relativistic geodesy [14].

The ^{229m}Th thorium isomer decays to the ground state primarily via internal conversion (IC) or photoemission. These two decay channels have vastly different timescales. The photoemission channel, which emits vacuum ultraviolet (VUV) photons, has a half-life of 1740(50)s [15]. This value for the vacuum half-life is based upon lifetime measurements in CaF2, a VUV transparent crystal that suppresses the IC decay channel. In these crystals the half-life is reduced due to the increased photon density of states in a dielectric, by a factor equal to the index of refraction cubed. The half-life in CaF₂ is 630(15) s [7,15,16], and 568(24) s in LiSrAlF₆ [17]. Internal conversion occurs when the excited nucleus transfers energy to the electron cloud, ejecting a conversion electron, similar to the Auger effect. The IC half-life is 7(1) us for neutral ^{229m}Th [18–20], about eight orders of magnitude faster than photoemission. A third decay channel, bound internal conversion, does not play a significant role in the experiments discussed here.

Several measurements [15,17,21] of the thorium isomer transition frequency based upon the photoemission decay channel have been published recently. The most accurate reported value of 2 020 407 384 335(2) kHz, corresponding to 8.355 733 554 020(8) eV, was achieved with laser excitation of the isomer in a CaF₂ crystal, with the laser referenced to

^{*}Deceased.

[†]Present address: Lawrence Livermore National Laboratory, 7000 East Ave, Livermore, California 94550, USA.

[‡]Present address: Department of Electrical and Computer Engineering and Department of Physics, University of Alberta, Edmonton, Alberta T6G 1H9, Canada.

a ⁸⁷Sr-based optical atomic clock [22]. Because these measurements rely on decay via photoemission, the measurement cycles are relatively long (hundreds of seconds).

Here we present a method of direct detection of the energy released by the IC decay and show that this much faster method can be used to measure the isomer energy. The IC energy is deposited in a solid state, thermally sensitive superconducting nanowire, then the IC decay is detected with high quantum efficiency. Initially, we aimed to reach an uncertainty of 10 meV to aid laser-based searches for the isomer transition energy [23]. Compared to isomer detection based upon the photoemission channel, the use of the eight orders of magnitude faster IC decay channel may enable much faster measurement cycles. Other IC detection schemes require an electron to overcome a work function to leave a surface, which occurs with relatively low probability on order 10^{-2} or lower [24]. Compared to other IC detection schemes, the present method of embedding the isomer in the detector is capable of near unity detection efficiency, and here we show a lower bound of 0.6(14) detection efficiency.

II. EXPERIMENTAL PROCEDURE

Beams of ²²⁹Th³⁺ are generated as recoil ions from the α decay of a 290 kBq ²³³U source. The recoil ions are thermalized and collimated by an rf + dc ring-electrode funnel in He gas and transferred via a supersonic gas jet through a de Laval nozzle into a subsequent segmented radio-frequency quadrupole acting as ion guide and phase-space cooler. Then a quadrupole mass-separator (QMS) stage selects one particular ion species. Ions are extracted from the QMS with a focusing triode structure at room temperature and accelerated towards subsequent detection. The accelerating voltage determining the ion kinetic energy is tunable, and was set to 30 V. This ion beamline was previously used with a microchannel plate detector for the first direct detection of the thorium isomer and with a magnetic bottle spectrometer to measure the isomer energy based on the kinetic energy of recoil electrons [25,26]. Null experiments are performed by selecting ions without the isomeric state such as ²³³U³⁺ with the same source and 230 Th^{2+,3+} with a ²³⁴U source.

The beamline directs ions onto the surface of superconducting nanowire sensors cooled to 2.7 K in a cryostat via a line-of-sight coupling, a schematic is shown in Fig. 1. Superconducting nanowire sensors are narrow superconducting wires biased near their critical current [27]. When a sufficient amount of energy is deposited, the critical current within a hot spot is reduced below the actual current and the device is driven into the normal resistive state [28,28,29]. This event results in a mV scale pulse. The typical recovery time of ≈ns is much shorter than the internal conversion lifetime of the Th isomer. Superconducting nanowire sensors typically operate at 3 K or below, and are the fastest single-photon sensors on record, with multiple independent reports of sub-10 ps jitter for photons of energy ≈ 1 eV [30,31]. While nanowires are more commonly used with the less energetic visible and infrared wavelengths, they have also been used with ions [32], ultraviolet photons [33], and x-rays [34]. The ions travel through 2 mm diameter line-of-sight holes in the 3 K and 40 K

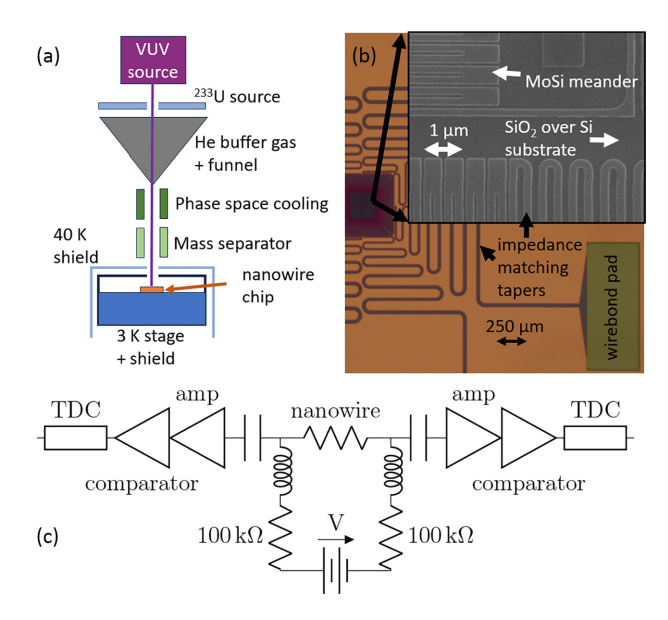


FIG. 1. (a) Schematic of ion beamline with nanowire sensors, not to scale. Recoil ions from a radioactive ^{233}U source are thermalized and collected by an rf + dc funnel in a buffer He gas, transferred through a de Laval supersonic nozzle into a segmented rf quadrupole acting as ion guide and phase-space cooler, then mass filtered in a quadrupole mass separator, finally accelerated towards the nanowire detectors mounted in a cryostat. The nanowires are positioned 10 mm from the QMS extraction electrodes; they are mounted on the 3 K stage, and the cryostat has two cryogenic shields at nominally 40 K and 3 K with 2 mm diameter holes to provide a line-of-sight path for ions. The calibration VUV source, a deuterium lamp with a grating monochromator, is located behind the radioactive source ≈ 1 m from the nanowire. The radioactive source has a small central hole to allow light to be sent through on axis. (b) Optical image of a portion of the nanowire chip with four nanowire delay-line imagers with inset scanning electron microscope image. Two of the imagers were read out simultaneously. (c) Delay-line readout circuit consisting of a nanowire with a differential bias applied with two room-temperature bias tees and a battery-powered voltage source. The signal from each side is amplified with a 1 GHz bandwidth amplifier then fed into a comparator then a time-to-digital converter (TDC).

shields of the cryostat to reach the nanowires. A deuterium lamp with a grating monochromator mounted on axis behind the radioactive source can irradiate the nanowire sensor with VUV photons with an energy known to one part in $\approx\!4000$. These VUV photons are used to calibrate the energy response of the nanowire sensor.

Energy resolution is achieved by exploiting the bias current dependence of the internal quantum efficiency of the nanowire sensor [35]. We assume identical response to energy from IC events and photoelectric absorption of VUV photons when both are absorbed in the nanowire because both events appear similar on a microscopic level; both events should result in a single energetic electron, then follow the same relaxation processes. Some rare-event searches and applications in radionuclide analysis use similarly embedded radioactive material in cryogenic thermal sensors for spectroscopy on keV to MeV energy depositions [36–39].

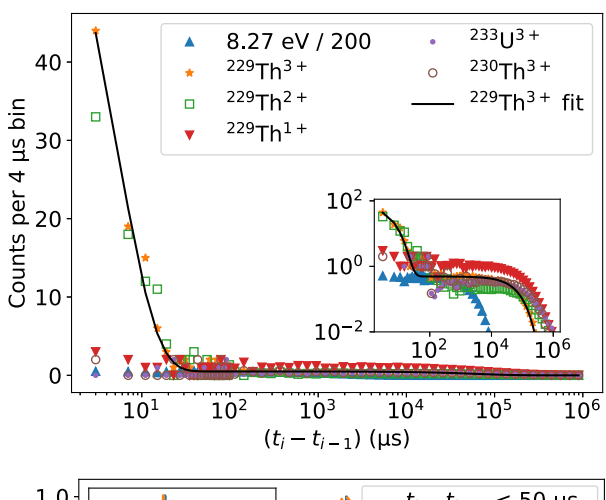
The nanowire sensor is a delay-line imager made of MoSi with a meander of width 180 nm [40]. Each imager fills a 100 µm square with fill fraction 0.7. The superconducting transition temperature is \approx 5 K. The nanowire was fabricated on a Si wafer; first a Ti-Au-Ti (2 nm-50 nm-2 nm) ground plane was deposited, then a 200 nm SiO₂ insulating layer, finally the 7.7 nm MoSi layer was deposited, capped with 2 nm sputtered Si, and patterned. Some of the capping Si likely alloys with the MoSi, and some likely oxidizes to SiO₂. The meander is both wider and thicker than typical superconducting nanowires, to increase the dependence of internal quantum efficiency on bias in the 8.4 eV energy range. For each event, we read out voltage pulses from both sides of the nanowire and record a timestamp for each pulse using the circuit shown in Fig. 1(c). The difference in the timestamps of the two pulses caused by a single event provides a measurement of the event location along the length of the nanowire. The timestamp of the *i*th event is $t_i = (t_{ia} + t_{ib})/2$ and the position is $x_i = 50(t_{ia} - t_{ib})/c$ where t_{ia} and t_{ib} are the timestamps from the two sides of the imager for event i, c is the speed of light, and the electrical propagation velocity in the nanowire is $\approx c/50$.

Some ions will stop in the capping layer rather than in the nanowire. We used the Stopping Range of Ions in Matter (SRIM 2013 [41]) software to calculate an ion stopping range of 2.2 nm in Si with density 2.05 g/cm³, with a fraction 0.75 of ions passing through a 2 nm layer. The density is lower than bulk Si due to the sputter deposition [42], the stopping range is similar for SiO₂ and MoSi, the other forms the capping layer may take. When energy is deposited in the capping layer, only a fraction of that energy will be detected by the nanowire, leading to reduced detection probability. The IC energy is near the detection threshold, while the ion kinetic energy is well above the detection threshold, so the detection probability of IC events will be affected more than ion events. When IC occurs in the capping layer the energy relaxation and transport takes place over the time range of picoseconds to nanoseconds, and thus any added delay is negligible compared to the IC decay half-life and does not change the time-correlation statistics.

III. RESULTS

Both the initial ion impact and the IC decay deposit energy into the detector, with the time separation being set by the IC half-life of \approx 7 μs . The energy deposition from ion impact and IC decay occurs at the same physical location. This ion impact and internal conversion coincidence presents two signatures in the data, a time correlation and a spatial correlation. These signatures only appear for ions which are known to sustain the isomer state which are $^{229}Th^{\geqslant 2+}$. Figure 2 (top) shows that time correlation is present for these ions, and is not present for other tested ions or photons. This rules out spurious sources of time correlation. The distribution of time differences is fit with the sum of two exponential distributions, one for the isomer events and one for the ion events.

Figure 2 (bottom) shows the spatial correlation observed for time-correlated events with ²²⁹Th³⁺ ions, and shows that spatial correlation is not present for time-separated events.



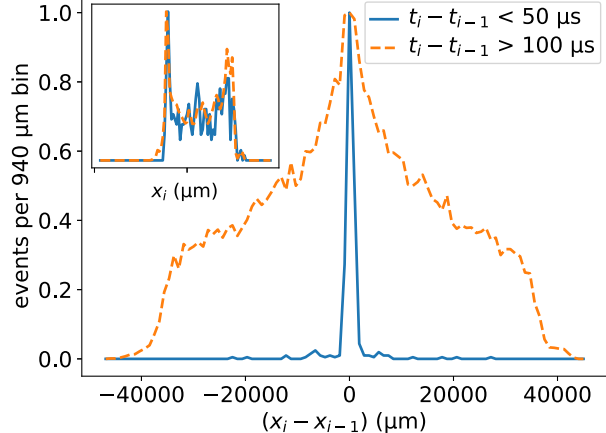


FIG. 2. (Top) The distribution of time differences between successive nanowire events for 8.27 eV (150 nm) photons and for various ions incident on the nanowires. The photon data duration is 100 s, the counts were divided by 200 to fit on the same scale as the ion data. The ion data duration is 3600 s and in each case was taken shortly after cooling the cryostat from room temperature. Timecorrelated events with sub 50 µs separation are present for ²²⁹Th^{2+,3+} and not present for any other ions including ²³⁰Th³⁺ or the photon data. Bin sizes are 4 µs before 100 µs and increase logarithmically after. A two-exponential fit to the ²²⁹Th³⁺ data with isomer half-life $7.9~\mu s$ and isomer fraction 1.2% is shown. Inset shows the same data and fit with a logarithmic vertical axis. (Bottom) Position difference between successive time-correlated ($t_i - t_{i-1} < 50 \,\mu s$) events and time-separated ($t_i - t_{i-1} > 100 \,\mu s$) events for ²²⁹Th³⁺, normalized to have a maximum value of 1. Time-correlated events show spatial correlation, while time-separated events do not. Inset, with y axis matching the primary figure, shows the distribution of positions, showing a nonuniform distribution with excess events at the edges. The nonuniformity may be due to pulse rise-time variation with position along the nanowire.

The observation of both time correlation and spatial correlation in the expected cases, and the lack of these signatures in null experiments, confirms the observation of thorium isomer IC decays.

The *isomer fraction* is the fraction of ion events followed by an isomer event $N_{\text{isomer}}/N_{\text{ion}}$, where N_{isomer} is the number of isomer events, $N_{\text{ion}} = N_{\text{total}} - N_{\text{isomer}}$ is the number of ion

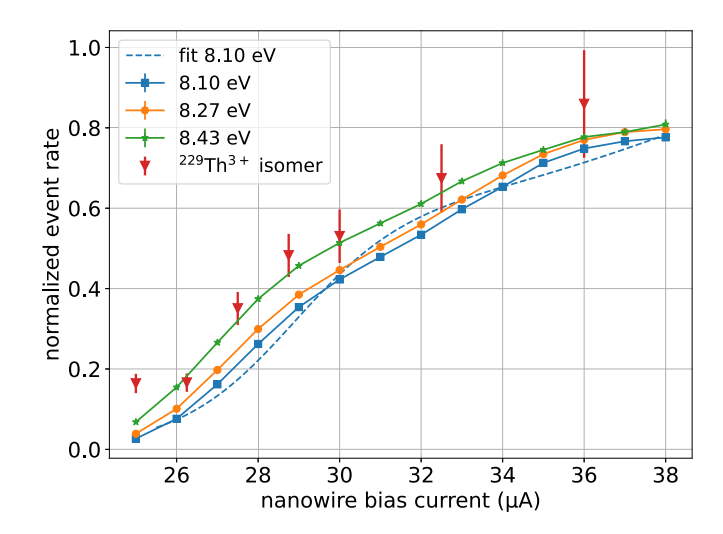


FIG. 3. Event rate vs nanowire bias current for three photon energies and for isomer decays, normalized by A in the fit described in the text. A fit of Eq. (1) to the 8.10 eV photon data is shown. Events with time separation less than 50 μ s are counted as isomer events, $x_i - x_{i-1}$ is not used to select isomer events because the position resolution degrades at lower current bias. Relative uncertainty on each point is given by $1/\sqrt{N}$ where N is the number of events. The nanowire bias was cycled repeatedly throughout this duration with a dwell time for each bias chosen to achieve a similar number of isomer counts per bias. There were ≈ 60 isomer counts per bias, leading to a roughly 1 part in 8 uncertainty on the relative intensity.

events, and N_{total} is the total number of events. We calculate N_{isomer} as number of events that are both time $(t_i - t_{i-1} < 50 \, \mu\text{s})$ and space $(x_i - x_{i-1} < 3000 \, \mu\text{m})$ correlated, and also determine N_{isomer} from the fit to the time differences. The results agree between the two methods. In these data we find an isomer fraction of 1.25(1)% and an IC half-life of 7.9 μ s. The isomer state is populated by a 2.1(5)% decay branch [43,44]. From this we obtain a lower limit on quantum efficiency for IC detection with the nanowire of 0.60(14).

Nanowire detectors achieve statistical energy resolution by exploiting the dependence of internal quantum efficiency on bias current. An energy resolution exceeding one part in 500 has been demonstrated in the detection of ≈ 0.8 eV photons [35]. We perform an analysis assuming monochromatic incident spectra for both photons and IC events. To calibrate the energy scale we illuminate the nanowire sensor with VUV light generated with a deuterium lamp, monochromatized with a grating, and measured the count rate as a function of the current bias for many wavelengths and for IC events.

Figure 3 shows normalized event rate vs current bias data for VUV photons and isomer events. The internal quantum efficiency of the nanowire increases from zero to, ideally, a maximum value known as *saturated absorption* with increased current bias. The maximum current bias is limited by latching current, for which an event drives the nanowire normal and it does not self-reset to the superconducting state. We did not observe saturated absorption, likely because the cross section of the nanowires is too large. The internal quantum efficiency of a nanowire is often well modeled with a single sigmoid [45,46]. The sigmoid shape is predicted based

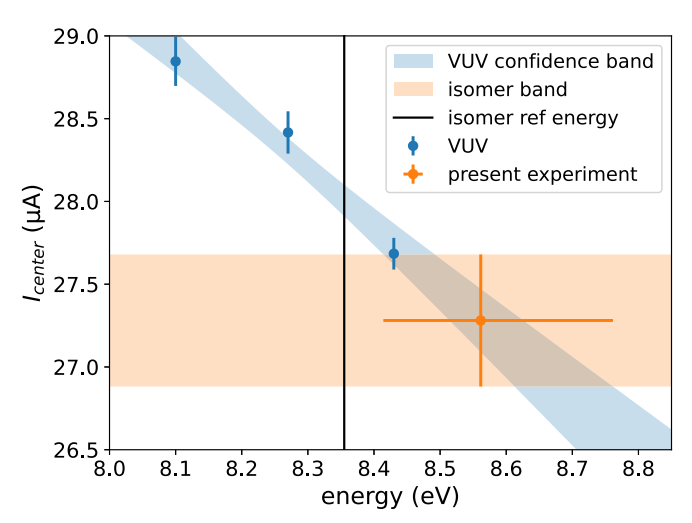


FIG. 4. I_{center} determined from fits of q(I) to the data in Fig. 3 vs energy. The isomer energy is determined from a linear fit to the 3 VUV points. A 1- σ confidence band is shown for that linear fit, and an isomer band is shown based on the uncertainty in the fit for I_{center} for the isomer data. The isomer energy statistical uncertainty is taken to be the range where the isomer band and the VUV confidence band overlap. The best value of isomer energy, the ref energy [22], is shown.

on Fano fluctuations of deposited energy that remains in the hotspot [47], and the width of the sigmoid will increase with deposited energy. Here, one sigmoid provides a very poor fit and we use two sigmoids to improve the quality of fit, one contributing factor may be critical current variation along the 40 mm imagers vs the 1 mm length typical for the cited nanowires; even two sigmoids do not provide a very good fit. We fit the data with

$$q(I) = A[(1 - f)z(i_1) + fz(i_2)], \tag{1}$$

where $z(i) = 1/(1 + e^{-i})$ is the sigmoid function, A is the event rate at saturated absorption, $i_1 = (I - I_{center})/I_{scale}$ is the normalized bias current. The second-term normalized bias current $i_2 = (I - 1.3I_{center})/(2I_{scale})$ has constants chosen to give a better quality of fit. When f = 0 then I_{center} is the magnitude of bias current at which the event rate is A/2, I_{center} will decrease with increasing event energy. The constants f = 0.4, $I_{\text{scale}} = 1.2 \,\mu\text{A}$ provide the best fit to the 8.10 eV photon data. To determine the isomer energy both A and I_{center} are determined with fits to the data in Fig. 3. Then a linear fit to I_{center} vs photon energy is used to convert the isomer I_{center} to energy. The statistical uncertainty of the isomer energy is taken to be the range of overlap between the confidence band of that linear fit and the isomer I_{center} uncertainty. Figure 4 shows this analysis and yields an isomer energy of $8.54^{+0.21}_{-0.16}$ eV for the data shown and $8.79_{-0.24}^{+0.31}$ eV for a second nominally identical nanowire recording data at the same time.

To estimate the systematic uncertainty we consider repeat analyses of the same data with significant modifications to the function q(I). We modified q(I) in the following ways; z(i) = (erf(i) + 1)/2, varying f from 0 to 1, and varying I_{scale} by a factor of 2 larger or smaller, the isomer energy varies by

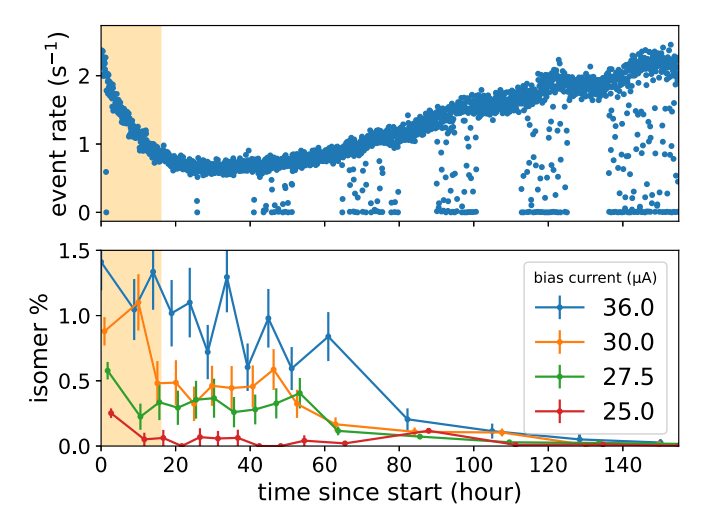


FIG. 5. (Top) Total event rate vs time, each point represents 4 minutes. Long-term drift and ion dropout periods are visible. (Bottom) Isomer fraction as percent over the same duration for various current biases. A decay of isomer fraction over time is visible. Orange bands show the time range used for the analyses in Figs. 3 and 4.

0.07 eV. To estimate the effect of nonmonochromatic lower-energy events either during calibration with VUV photons or IC events where some energy is lost in the capping layer, we repeat the analysis setting f to zero only when fitting the calibration data or only when fitting the isomer data. The difference between these two cases is 0.11 eV. We perform a weighted average of the results from the two nanowires, taking the statistical uncertainty to be the larger of the asymmetric uncertainties. We take the systematic uncertainty to be the quadrature sum of the two terms in this paragraph. We arrive at an isomer energy of $8.6(2_{\rm stat})(1_{\rm sys})$ eV.

The measurement apparatus has some instability, likely due to the accumulation of charge on insulating surfaces and frozen gasses on the surface of the nanowire sensor. Figure 5 shows the total event rate and isomer fraction vs time for the isomer data. The total event rate shows both a gradual variation and occasional periods of ion signal dropouts, which we attribute to charge accumulation on insulating surfaces due to the relatively fast timescales and nonmonotonic behavior. The ion dropouts are not due to latching. During an ion dropout the nanowires remain sensitive to VUV photons, and the ion signal does not return upon resetting the bias to zero and back. The count rate during ion dropouts places an upper limit on the dark-count rate, count rates of 0.01 Hz and lower were observed for all biases. The dark-count rates are low enough to have a negligible effect on our results. The isomer fraction degrades by a factor of 7 over 100 hours, which is likely due to frozen gas accumulation. We consider the hypothesis that the primary frozen gas is water, and the isomer signal is missing because the ice slows the ions such that they stop in the Si capping layer. In a SRIM calculation of 90 eV ²²⁹Th ions incident on 1 nm of ice followed by the 2 nm Si capping layer, a fraction 0.12 of ions reach the nanowire, 6.2 times less compared to no ice. This model for isomer fraction decay suggests an ice accumulation rate of ≈ 0.01 nm/hour.

Both effects appear to be reset upon warming the cryostat to room temperature and cooling back to base temperature, so all data were taken shortly after a warmup-cooldown. The typical pressure measured near the cryostat was 5×10^{-7} bar near room temperature and 4×10^{-8} bar near base temperature.

IV. DISCUSSION

The energy measurement made with this apparatus could be improved significantly by mitigating some of the issues noted in this manuscript and improved counting statistics. Eliminating line-of-sight from the nanowires to room temperature would significantly reduce frozen gas accumulation, and could potentially be achieved with a cryogenically cooled ion-bender-based coupling scheme or a liquid-helium-based method for slowing the recoil ions. The charge buildup may be mitigated by reducing the interaction between ions and insulating material; for example, the nanowires could be fabricated on a conductive substrate and could be made with a conductive capping layer. The calibration would be improved by using more photon energies and bias points. There are likely some amount of lower-energy photons reaching the nanowire sensor, primarily from VUV-excited fluorescence from nearby materials such as the SiO2, Si, and any frozen gasses. With additional characterization of the nanowire response to photons over a wide energy range, and using the methods in Ref. [35], the full incident-photon spectrum could be resolved and accounted for in the analysis. VUV calibration curves taken 3 days apart without a warmup-cooldown cycle in between agree at the 0.01 eV level, so fluorescence from frozen gasses do not appear to have a large effect on the VUV response. The uncertainty related to ions stopping in the capping layer could be reduced with a thinner capping layer and a larger accelerating voltage. Understanding the reason for and eliminating the nonsigmoid shape of the count rate vs bias would be beneficial, potential approaches include methods to study position dependence in nanowires [32,48] and characterization of detectors with different dimensions.

Improved sensitivity could be obtained with fewer isomer events by using a sensor with single-event energy resolution. One potential such sensor is the optical transition edge sensor microcalorimeter [49]. A 1σ energy resolution of 0.1 eV or better is regularly achieved for energies up to 10 eV, and small signal recovery times can be below 1 us. The recovery time will be longer for ion impacts with energies $\gg 10 \text{ eV}$ due to saturation of the device, but can still be kept below the IC lifetime [50,51]. Using such a device, the precision scales as σ/\sqrt{N} , where σ is the one standard-deviation energy resolution and N is the number of IC decays observed. With such a detector, 0.01 eV precision would require only 100 observed IC events. These events could be collected in less than one hour, based upon the count rates observed in the present device scaled to a 50 µm square sensor. Events of significantly different energy would be easily distinguished and not affect the energy measurement. The absorbing material can be Au, free of surface oxide, which would make the physics of IC and photon absorption even more similar due to the lack of capping layer. Calibration can be achieved by absorption of nlow-energy photons of known energy nearly simultaneously.

The primary challenge in using such a sensor is that they require ≈ 0.1 K temperatures, which puts greater demands on the ion coupling scheme to minimize thermal loads on the sensor and requires a more elaborate cryostat. Some efforts in this direction are reported in Ref. [52]. A measurement of the 76.737(18) eV 235m U nuclear isomer was made with a similar sensor known as a superconducting tunnel-junction (STJ) sensor and with a photon-counting-based calibration. The STJ sensor had 50 μ s recovery time, slower than the IC half-life of Th^{m229} case but much faster than the 235m U IC half-life of 26 minutes [53].

To conclude, we present a method of direct detection of thorium isomers via the IC decay channel by embedding ^{229m}Th in a superconducting nanowire sensor. We measure an isomer energy of $8.6(2_{stat})(1_{sys})$ eV via the dependence of internal quantum efficiency on bias current, consistent with the best available value of 8.36 eV. We argue that the ability to detect thorium isomer populations via internal conversion may provide value due to the combination of fast measurement cycles and high quantum efficiency, perhaps for use in an internal conversion-based nuclear clock [54]. A device consisting of nanowire with a low energy threshold (0.2 eV has been demonstrated [55]) with a layer of ²²⁹ThO₂ deposited

on top should be capable of both laser excitation of the isomer state and nanowire detection of the IC decay even when the conversion electron scatters a few times before reaching the nanowire.

ACKNOWLEDGMENTS

This work is part of the "ThoriumNuclearClock" project that received funding from the European Research Council (ERC) under the European Union's Horizon 2020 Research and Innovation Programme (Grant Agreement No. 856415) and of the European Union's Horizon 2020 Research and Innovation Programme 'nuClock' (Grant Agreement No. 664732). The work at NIST is supported by the U.S. Department of Energy, Office of Science, Office of Nuclear Physics under Award No. DE-SC0021368. We thank Dr. Laura Sinclair for facilitating initial connections between some coauthors. Work in JILA was supported by Army Research Office Grant No. W911NF-2010182.

DATA AVAILABILITY

The data that support the findings of this article are openly available [56].

- [1] E. Peik and C. Tamm, Europhys. Lett. 61, 181 (2003).
- [2] C. J. Campbell, A. G. Radnaev, A. Kuzmich, V. A. Dzuba, V. V. Flambaum, and A. Derevianko, Phys. Rev. Lett. 108, 120802 (2012).
- [3] K. Beloy, Phys. Rev. Lett. 130, 103201 (2023).
- [4] V. V. Flambaum, Phys. Rev. Lett. 97, 092502 (2006).
- [5] L. von der Wense, B. Seiferle, and P. G. Thirolf, Meas. Tech. 60, 1178 (2018).
- [6] E. Peik and M. Okhapkin, C. R. Phys. 16, 516 (2015).
- [7] K. Beeks, T. Sikorsky, T. Schumm, J. Thielking, M. V. Okhapkin, and E. Peik, Nat. Rev. Phys. 3, 238 (2021).
- [8] W. G. Rellergert, D. DeMille, R. R. Greco, M. P. Hehlen, J. R. Torgerson, and E. R. Hudson, Phys. Rev. Lett. 104, 200802 (2010).
- [9] A. Derevianko and M. Pospelov, Nat. Phys. 10, 933 (2014).
- [10] A. Arvanitaki, S. Dimopoulos, V. Gorbenko, J. Huang, and K. Van Tilburg, J. High Energy Phys. 05 (2017) 071.
- [11] K. Van Tilburg, N. Leefer, L. Bougas, and D. Budker, Phys. Rev. Lett. 115, 011802 (2015).
- [12] A. Hees, J. Guéna, M. Abgrall, S. Bize, and P. Wolf, Phys. Rev. Lett. 117, 061301 (2016).
- [13] Y. V. Stadnik, Phys. Rev. D 102, 115016 (2020).
- [14] A. Kulosa, T. Mehlstäubler, E. Peik, P. Schmidt, and A. Surzhykov, PTB Commun. 128, 27 (2018).
- [15] J. Tiedau, M. Okhapkin, K. Zhang, J. Thielking, G. Zitzer, E. Peik, F. Schaden, T. Pronebner, I. Morawetz, L. T. De Col, F. Schneider, A. Leitner, M. Pressler, G. Kazakov, K. Beeks, T. Sikorsky, and T. Schumm, Phys. Rev. Lett. 132, 182501 (2024).
- [16] A. Yamaguchi, Y. Shigekawa, H. Haba, H. Kikunaga, K. Shirasaki, M. Wada, and H. Katori, Nature (London) 629, 62 (2024).
- [17] R. Elwell, C. Schneider, J. Jeet, J. E. Terhune, H. W. Morgan, A. N. Alexandrova, H. B. Tran Tan, A. Derevianko, and E. R. Hudson, Phys. Rev. Lett. 133, 013201 (2024).

- [18] B. Seiferle, L. von der Wense, and P. G. Thirolf, Phys. Rev. Lett. 118, 042501 (2017).
- [19] E. V. Tkalya, C. Schneider, J. Jeet, and E. R. Hudson, Phys. Rev. C 92, 054324 (2015).
- [20] E. V. Tkalya, C. Schneider, J. Jeet, and E. R. Hudson, Phys. Rev. C **95**, 039902(E) (2017).
- [21] S. Kraemer, J. Moens, M. Athanasakis-Kaklamanakis, S. Bara, K. Beeks, P. Chhetri, K. Chrysalidis, A. Claessens, T. E. Cocolios, J. G. Correia, H. D. Witte, R. Ferrer, S. Geldhof, R. Heinke, N. Hosseini, M. Huyse, U. Köster, Y. Kudryavtsev, M. Laatiaoui, R. Lica et al., Nature (London) 617, 706 (2023).
- [22] C. Zhang, T. Ooi, J. S. Higgins, J. F. Doyle, L. von der Wense, K. Beeks, A. Leitner, G. A. Kazakov, P. Li, P. G. Thirolf, T. Schumm, and J. Ye, Nature (London) 633, 63 (2024).
- [23] L. C. von der Wense, B. Seiferle, C. Schneider, J. Jeet, I. Amersdorffer, N. Arlt, F. Zacherl, R. Haas, D. Renisch, P. Mosel, P. Mosel, M. Kovacev, U. Morgner, C. E. Düllmann, E. R. Hudson, and P. G. Thirolf, Hyperfine Interact. 240, 23 (2019).
- [24] L. von der Wense, B. Seiferle, S. Stellmer, J. Weitenberg, G. Kazakov, A. Pálffy, and P. G. Thirolf, Phys. Rev. Lett. 119, 132503 (2017).
- [25] L. von der Wense, B. Seiferle, M. Laatiaoui, J. B. Neumayr, H.-J. Maier, H.-F. Wirth, C. Mokry, J. Runke, K. Eberhardt, C. E. Düllmann, N. G. Trautmann, and P. G. Thirolf, Nature (London) 533, 47 (2016).
- [26] B. Seiferle, L. von der Wense, P. V. Bilous, I. Amersdorffer, C. Lemell, F. Libisch, S. Stellmer, T. Schumm, C. E. Düllmann, A. Pálffy, and P. G. Thirolf, Nature (London) 573, 243 (2019).
- [27] C. M. Natarajan, M. G. Tanner, and R. H. Hadfield, Supercond. Sci. Technol. 25, 063001 (2012).
- [28] A. Simon, R. Foster, M. Sahoo, J. Shi, E. Batson, F. Incalza, M. Castellani, O. Medeiros, C. Heil, and K. K. Berggren, arXiv:2501.13791.

- [29] J. Allmaras, A. Kozorezov, B. Korzh, K. Berggren, and M. Shaw, Phys. Rev. Appl. 11, 034062 (2019).
- [30] B. Korzh, Q. Y. Zhao, J. P. Allmaras, S. Frasca, T. M. Autry, E. A. Bersin, A. D. Beyer, R. M. Briggs, B. Bumble, M. Colangelo, G. M. Crouch, A. E. Dane, T. Gerrits, A. E. Lita, F. Marsili, G. Moody, C. Peña, E. Ramirez, J. D. Rezac, N. Sinclair et al., Nat. Photon. 14, 250 (2020).
- [31] M. Colangelo, B. Korzh, J. P. Allmaras, A. D. Beyer, A. S. Mueller, R. M. Briggs, B. Bumble, M. Runyan, M. J. Stevens, A. N. McCaughan, D. Zhu, S. Smith, W. Becker, L. Narváez, J. C. Bienfang, S. Frasca, A. E. Velasco, C. H. Peña, E. E. Ramirez, A. B. Walter *et al.*, Phys. Rev. Appl. 19, 044093 (2023).
- [32] C. Peña, C. Wang, S. Xie, A. Bornheim, M. Barría, C. S. Martín, V. Vega, A. Apresyan, E. Knehr, B. Korzh, J. Luskin, L. Narváez, S. Patel, M. Shaw, and M. Spiropulu, JINST 20, P03001 (2025).
- [33] E. E. Wollman, V. B. Verma, A. D. Beyer, R. M. Briggs, B. Korzh, J. P. Allmaras, F. Marsili, A. E. Lita, R. P. Mirin, S. W. Nam, and M. D. Shaw, Opt. Express 25, 26792 (2017).
- [34] K. Inderbitzin, A. Engel, A. Schilling, K. Ilin, and M. Siegel, Appl. Phys. Lett. 101, 162601 (2012).
- [35] L. Kong, Q. Zhao, H. Wang, J. Guo, H. Lu, H. Hao, S. Guo, X. Tu, L. Zhang, X. Jia, L. Kang, X. Wu, J. Chen, and P. Wu, Nano Lett. 21, 9625 (2021).
- [36] R. P. Fitzgerald, B. K. Alpert, D. T. Becker, D. E. Bergeron, R. M. Essex, K. Morgan, S. Nour, G. O'Neil, D. R. Schmidt, G. A. Shaw, D. Swetz, R. M. Verkouteren, and D. Yan, J. Res. Natl. Inst. Stand. Technol. 126, 126048 (2021).
- [37] M. Griedel, F. Mantegazzini, A. Barth, E. Bruer, W. Holzmann, R. Hammann, D. Hengstler, N. Kovac, C. Velte, T. Wickenhäuser, A. Fleischmann, C. Enss, L. Gastaldo, H. Dorrer, T. Kieck, N. Kneip, C. E. Düllmann, and K. Wendt, J. Low Temp. Phys. 209, 779 (2022).
- [38] B. K. Alpert, M. Balata, D. T. Becker, D. A. Bennett, M. Borghesi, P. Campana, R. Carobene, M. De Gerone, W. B. Doriese, M. Faverzani, L. Ferrari Barusso, E. Ferri, J. W. Fowler, G. Gallucci, S. Gamba, J. D. Gard, F. Gatti, A. Giachero, M. Gobbo, U. Köster et al., arXiv:2503.19920.
- [39] A. S. Hoover, E. M. Bond, M. P. Croce, T. G. Holesinger, G. J. Kunde, M. W. Rabin, L. E. Wolfsberg, D. A. Bennett, J. P. Hays-Wehle, D. R. Schmidt, D. Swetz, and J. N. Ullom, Anal. Chem. 87, 3996 (2015).

- [40] Q. Y. Zhao, D. Zhu, N. Calandri, A. E. Dane, A. N. McCaughan, F. Bellei, H. Z. Wang, D. F. Santavicca, and K. K. Berggren, Nat. Photon. 11, 247 (2017).
- [41] J. F. Ziegler, M. Ziegler, and J. Biersack, Nucl. Instrum. Methods Phys. Res. Sect. B 268, 1818 (2010).
- [42] W. T. Pawlewicz, J. Appl. Phys. 49, 5595 (1978).
- [43] J. Thielking, M. V. Okhapkin, P. Głowacki, D. M. Meier, L. Von Der Wense, B. Seiferle, C. E. Düllmann, P. G. Thirolf, and E. Peik, Nature (London) 556, 321 (2018).
- [44] V. Barci, G. Ardisson, G. Barci-Funel, B. Weiss, O. El Samad, and R. K. Sheline, Phys. Rev. C 68, 034329 (2003).
- [45] T. Yamashita, S. Miki, H. Terai, and Z. Wang, Opt. Express 21, 27177 (2013).
- [46] W. J. Zhang, H. Li, L. X. You, J. Huang, Y. H. He, L. Zhang, X. Y. Liu, S. J. Chen, Z. Wang, and X. M. Xie, IEEE Photonics J. 8, (2016).
- [47] A. G. Kozorezov, C. Lambert, F. Marsili, M. J. Stevens, V. B. Verma, J. P. Allmaras, M. D. Shaw, R. P. Mirin, and S. W. Nam, Phys. Rev. B 96, 054507 (2017).
- [48] X. Zhang, X. Zhang, J. Huang, C. Yang, L. You, X. Liu, P. Hu, Y. Xiao, W. Zhang, Y. Wang, L. Li, Z. Wang, and H. Li, Superconductivity 1, 100006 (2022).
- [49] A. E. Lita, A. J. Miller, and S. W. Nam, Opt. Express 16, 3032 (2008).
- [50] T. Gerrits, B. Calkins, N. Tomlin, A. E. Lita, A. Migdall, R. Mirin, and S. W. Nam, Opt. Express 20, 23798 (2012).
- [51] B. Calkins, A. E. Lita, A. E. Fox, and S. Woo Nam, Appl. Phys. Lett. 99, 241114 (2011).
- [52] M. Fedkevych, M. Biasotti, M. De Gerone, L. Ferrari Barusso, G. Gallucci, F. Gatti, M. Giovannini, M. Osipenko, M. Ripani, and B. Siri, IEEE Trans. Appl. Supercond. 31, 1 (2021).
- [53] F. Ponce, E. Swanberg, J. Burke, R. Henderson, and S. Friedrich, Phys. Rev. C 97, 054310 (2018).
- [54] L. von der Wense and C. Zhang, Eur. Phys. J. D 74, 146 (2020).
- [55] M. Colangelo, A. B. Walter, B. A. Korzh, E. Schmidt, B. Bumble, A. E. Lita, A. D. Beyer, J. P. Allmaras, R. M. Briggs, A. G. Kozorezov, E. E. Wollman, M. D. Shaw, and K. K. Berggren, Nano Lett. 22, 5667 (2022).
- [56] G. O'Neil, Data for "Direct detection of the \sim 8.4 eV internal conversion energy of 229mTh embedded in a superconducting nanowire", https://doi.org/10.18434/mds2-3835.